Triple-differential cross sections to discrete states in the $^{16}O(\pi^+,2p)^{14}N$ reaction

W. R. Wharton,* P. D. Barnes, B. Bassalleck,† R. A. Eisenstein,‡ G. Franklin, R. Grace, C. Maher, P. Pile,§ R. Rieder, and J. Szymanski
Carnegie-Mellon University, Pittsburgh, Pennsylvania 15213

J. R. Comfort
Arizona State University, Tempe, Arizona 85287

F. Takeutchi
Kyoto-Sangyo University, Kyoto 603, Japan

J. F. Amann
Los Alamos Scientific Laboratory, Los Alamos, New Mexico 87545

S. A. Dytman**
Massachusetts Institute of Technology, Cambridge, Massachusetts 02139

K. G. R. Doss††
University of Washington, Seattle, Washington 98195

(Received 10 October 1984)

The $^{16}O(\pi^+,2p)^{14}N$ reaction has been studied at $T_\pi = 59.6$ MeV. Good energy resolution of 1 to 2 MeV allows several states in ^{14}N to be resolved. Triple-differential cross sections are presented for the transitions to the ^{14}N 1^+ ground state and 1^+ 4 MeV state. The quasideuteron model is used to construct a T matrix for each transition. A fit to the data requires an additional term in the T matrix giving a large anisotropy in the angular distribution of the ^{14}N recoil momentum vector. The ground state T matrix has an unexpected enhancement near zero recoil momentum of the ^{14}N nucleus. The "measured" T matrices are then used to extrapolate to unmeasured regions of phase space giving double differential, single-differential, and total cross sections for each transition.

I. INTRODUCTION

Investigations of pion absorption in nuclei[1,2] play a crucial role in the development of pion-nuclear physics research. The understanding of the pion absorption mechanism is important to a more fundamental understanding of important parts of nuclear structure and the nucleon-nucleon interaction inside nuclei. This is related to the question[3] of how pion fields and the pion-nucleon coupling are modified in the presence of many nearby nucleons. Pion absorption is a major part of the pion-nucleus total reaction cross section, but is much less well understood than the other parts of the pion-nucleus interaction. Because the various reaction channels compete with, and thereby influence, each other, our poor knowledge of the pion absorption mechanism has adversely affected our understanding of the pion elastic, inelastic, and change exchange channels.[4] Pion absorption involves a large momentum transfer between nucleons, corresponding to short interaction distances ≤ 0.5 F. This region of nuclear physics is not understood and could be a place where the quark degrees of freedom manifest themselves.[5,6]

Differential cross sections of pion absorption to discrete channels in nuclei heavier than ^{3}He have only been measured for two-body final states, for example the $A(\pi^+,p)B$ reactions,[1] which account for only a fraction of a percent of the total absorption cross section. A much larger fraction of the absorption cross section is contained in the $A(\pi^+,2p)B$ reaction[7,8] for which triple-differential cross sections have not previously been measured for individual states. The simplest reliable pion absorption models describe absorption on a nucleon pair. These models can be most easily tested with the $A(\pi^+,2p)B$ reaction. The $(\pi^+,2p)$ reaction has typically one-fifth as large a momentum transfer to the residual nucleus as does the extensively studied (π^+,p) reaction. Therefore, it is thought that the nucleons in the final nucleus are less involved in the $(\pi^+,2p)$ reaction than in the (π^+,p) reaction.[1] The large momentum of the emitted protons in the $(\pi^+,2p)$ reaction can arise from the πNN interaction and does not require the high momentum tails of the nuclear wave functions to as great an extent as in the (π^+,p) reaction. With the primary goal of learning about the pion absorption process we have measured triple-differential cross sections at $T_\pi = 59.6$ MeV for the $^{16}O(\pi^+,2p)^{14}N$ reaction to the 1^+ g.s. and the 1^+ 3.95 MeV second excited state.

II. EXPERIMENTAL TECHNIQUE AND ANALYSIS PROCEDURE

The $^{16}O(\pi^+,2p)$ reaction was studied at the low-energy proton (LEP) channel at the Los Alamos Meson Physics Facility (LAMPF). A schematic of our detection system is shown in Fig. 1. The coincident proton energies were measured using two solid state spectrometers[9] constructed from stacks of high purity germanium crystals and lithium drifted silicon detectors placed at beam height. Because of a large beam spot on target, each detector scanned a horizontal angular range of about ± 12 deg and a vertical angular range of about ± 4.5 deg. In front of each spectrometer were individual-wire-readout proportional chambers which measured the direction of each proton's momentum to an accuracy varying from 0.5 to 2.0 deg. From the measured proton momenta the recoil momentum is calculated using conservation of momentum. The beam on target was monitored with two ionization chambers placed after the target. A more complete description of the apparatus and its performance is given elsewhere.[9–11]

Figure 2 shows missing mass spectra for the $^{16}O(\pi^+,2p)^{14}N$ reaction. The energy resolution for our spectra was 1.0—2.0 MeV FWHM, 3—4 times better than previous $(\pi,2N)$ measurements.[7,8,12] The four strongest states at 0.0, 3.95, 7.03, and 11.05 MeV are the four strongest states seen in the $^{16}O(d,^4He)^{14}N$ reaction.[13] This paper is restricted to the analysis of the 1^+ ground state and 3.95 MeV state. The target was liquid water, 90 mg/cm^2 thick, contained within two stretched sheets of 25 μm Mylar. The target nonuniformity, $\pm 8\%$, was monitored between data runs by measuring[14] the transmission of electrons from a ^{90}Sr source through the target. Five percent, by weight, of the target was D_2O. The

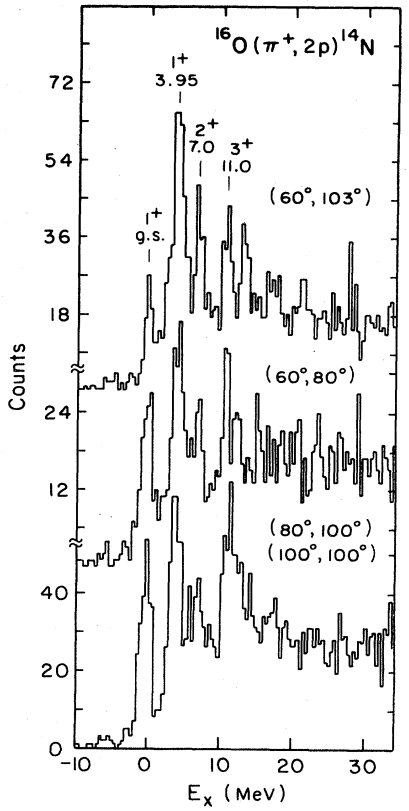

FIG. 2. ^{14}N spectra from the $^{16}O(\pi^+,2p)^{14}N$ reaction at $T_p = 59.6$ MeV. Only events with recoil momentum between 160 and 220 MeV/c are included. The three spectra were taken with different detector angles θ_1, θ_2: (60°,103°), (60°,80°), (80°,100°), and (100°,100°). The spectra at each pair of angles correspond to a different recoil momentum direction (see Table I).

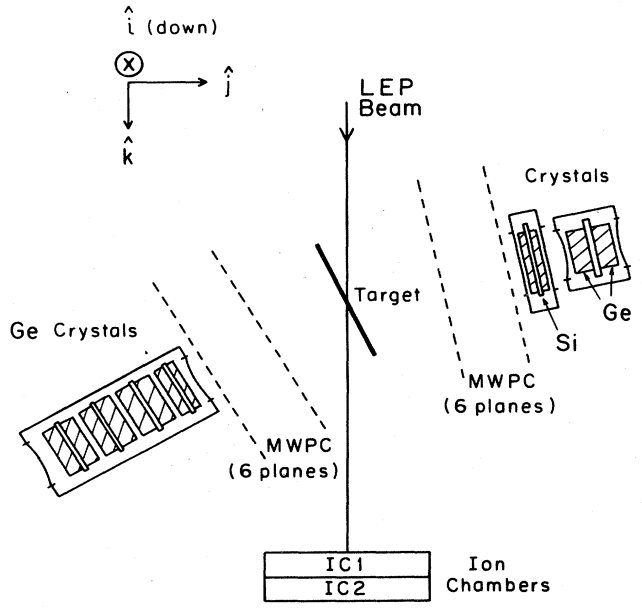

FIG. 1. A schematic of our detection system. The coordinate system used in the text is displayed in the upper left-hand corner.

$^{16}O(\pi^+,2p)^{14}N$ and $^2H(\pi^+,2p)$ reactions were measured simultaneously, with the data separated by the different Q values of the two reactions. The detection of both protons from the $^2H(\pi^+,2p)$ reaction allowed us to check the energy calibration of our detectors to within 100 keV, and check the opening angle between our two spectrometers to within 0.15°.

The extraction of cross sections from the data requires a careful mapping of the detection efficiency over the full phase-space acceptance of the detectors. For this purpose we have developed a Monte Carlo code which simulates every important feature of the experiment, including energy straggling, deadlayers between crystals, Moliere scattering, target nonuniformity, beam divergence, and measurement errors. These measurement errors, in both angle and energy, could be determined accurately by assuming all observed violations of energy and momentum conservation in the $^2H(\pi^+,2p)$ reaction are due to measurement errors. The centroids of the missing energy and momentum measured in the $^2H(\pi^+,2p)$ coincident measurement gave us very precise calibration points, whereas the widths of these distributions (which should be delta functions) gave us an excellent continuous monitor of all

sources of measurement errors. For a more complete description of this monitoring see Ref. 10.

Since there are three particles in the final state of the $^{16}O(\pi^+,2p)^{14}N$ reaction, nine coordinates are needed to specify the kinematics of each event, of which four are constrained by energy and momentum conservation. The remaining five variables are chosen to be, $\mathbf{P}_R$, the momentum of the recoiling nucleus, and (θ_1,ϕ_1), the angles of one of the two protons. The angle θ_1 is defined as the angle between the proton and the pion momentum direction, with ϕ_1 as the corresponding azimuthal angle. The Monte Carlo code is used to find the dependence of the T matrix upon these five variables for the $^{16}O(\pi^+,2p)^{14}N$ reaction to each discrete state.

The procedure is iterative. A reasonable functional form of $[T(\theta_1,\phi_1,\mathbf{P}_R)]^2$ is assumed in the calculation and the distributions of simulated events, calculated by the Monte Carlo code, are compared to the experimental distributions. We then adjust the parameters in the T matrix to try to fit the data. The iteration is repeated until all Monte Carlo simulated distributions agree with their corresponding experimentally measured distributions. The iteration process involves trying several functional forms for the T matrix. Because we can guess only a reasonable approximation of its functional form, the T matrix is not uniquely determined. This procedure allows us to extract and present all of our measured triple-differential cross sections in an efficient manner.

Once the Monte Carlo code simulates the $^{16}O(\pi^+,2p)$ experimental distributions, absolute cross sections can be obtained using the known $^2H(\pi^+,2p)$ cross sections which are represented by

$$d\sigma/d\Omega_1=(6.85/2\pi)[1+1.09P_2(\cos\theta_1)] \text{ mb/sr}$$

in the center of the mass. (For the most recent data on this reaction see Ref. 15.) This is accomplished by comparing the measured yields for each $^{16}O(\pi^+,2p)$ transition with the yield for the $^2H(\pi^+,2p)$ reaction and correcting for the coincidence-detection efficiencies as calculated by the Monte Carlo code. Data were taken at four sets of central detector angles: $(\theta_1,\theta_2)=(60°,80°)$, $(60°,103°)$, $(80°,100°)$, and $(100°,100°)$. The last pair of angles was too far from the $^2H(\pi^+,2p)$ two-body kinematics to detect these monitor events.

After the T matrix is normalized, the absolute value of the measured triple-differential cross sections is obtained. The triple-differential cross sections are most easily displayed as one-dimensional slices through the available phase space of the data. There is no simple efficient way to display the full multidimensional measured cross sections. Rather, we give all the information for the reader to calculate the triple differential cross sections which we measured. Any triple-differential cross section can be obtained from formulas similar to the following:

$$\frac{d^3\sigma}{dE_1 d\Omega_1 d\Omega_2}=\frac{1}{(2\pi)^5}\frac{E_\pi E_1 E_2 k_1 k_2}{k_\pi(1-\boldsymbol{\beta}_R\cdot\boldsymbol{\beta}_2/\beta_2^2)}|T|^2, \quad (1)$$

where the kinematic factor is expressed in terms of laboratory energies, wave numbers, and velocities of the pion (π), protons (1,2), and residual nucleus (R). T represents the transition matrix, which we now describe.

III. THE CHOICE OF THE T MATRIX

The functional form of the T matrix was chosen primarily on the basis of fitting the data. However, the quasideuteron model, in which the pion interacts exclusively with a proton-neutron pair in a $^3S_1$ relative state, gave us a reasonable start for our T matrix; providing the first two factors in the expression,

$$|T|^2=f(P_R)\times[1+a_2P_2(\cos\theta_1')]\times g(\theta_R,\phi_R). \quad (2)$$

Here all quantities are evaluated in the laboratory frame except for θ_1' which is evaluated in the center of momentum of the two protons. The first factor $f(P_R)$ is referred to as the form factor and is similar to form factors measured in other $(\pi,2N)$ experiments.[12] In the quasideuteron model, $f(P_R)$ is the absolute square of the momentum wave function of the quasideuteron center of mass in the target nucleus. The second factor is similar to the θ_1' dependence of the elementary $^2H(\pi^+,2p)$ cross section in the center-of-mass frame of this reaction. The third factor gives the dependence of the T matrix upon θ_R,ϕ_R. The quasideuteron model would predict only a weak θ_R dependence (as explained in the following) and would not predict any ϕ_R dependence.

It should be emphasized that everything in Eqs. (1) and (2) is evaluated in the laboratory frame except the θ_1' term. The phase space factor in Eq. (1) correctly includes the Jacobian which transforms the θ_1' angular dependence to the laboratory frame. In fact, this can be easily verified by setting $f(P_R)$ to the delta function $\delta(0)$, and integrating Eq. (1) over $dE_1 d\Omega_2$ to get $d\sigma/d\Omega_1$, which gives the $^2H(\pi^+,2p)$ angular distribution in the laboratory frame.

Before beginning the Monte Carlo analysis with a trial T matrix, consider the data which, in contradiction to the quasideuteron model, give very distinct evidence for a strong (θ_R,ϕ_R) dependence in the T matrix. Shown in Fig. 3 is the yield ratio of $(\pi^+,2p)$ events for populating the two 1^+ states (ground state/4 MeV state) plotted against recoil angle, θ_R, where

$$\cos\theta_R=\hat{\mathbf{P}}_R\cdot\hat{\mathbf{P}}_\pi,$$

$$\theta_R=0°\rightarrow 180° \text{ for } \mathbf{P}_R\cdot\hat{\mathbf{j}}>0$$

$$=180°\rightarrow 360° \text{ for } \mathbf{P}_R\cdot\hat{\mathbf{j}}<0.$$

Here, $\hat{\mathbf{j}}$ is the unit vector shown in Fig. 1, such that a rotation $\theta_R=0°\rightarrow 360°$ is counterclockwise in the figure. The reason for taking the ratio of events for these two 1^+ states is that any detection bias is factored out. The observed ratio is not isotropic in θ_R, indicating that either one or both of these two transitions must have a (θ_R,ϕ_R) dependence in the T matrix. A ϕ_R dependence is also necessary because the distribution in Fig. 3 is not symmetric about 180°. After proceeding with the Monte Carlo simulation of our experiment, we found that both transitions needed a strong (θ_R,ϕ_R) dependence in the T matrix.

Figure 3 gives us a clue about the form of $g(\theta_R,\phi_R)$ to use in the T matrix. For most of these data the two proton detectors were centered at $\theta=100°$ and 300°. Figure 3, which includes the data for recoil momenta larger than

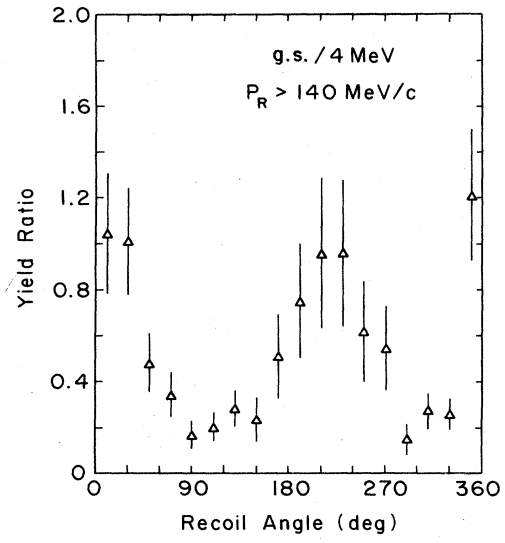

FIG. 3. The ratio of the experimental yields of the two 1^+ states (ground state/4 MeV state), plotted against recoil angle. The angle is defined in the text. The data are from all detector angles used in the experiment, but are restricted to events with recoil momentum greater than 140 MeV/c.

140 Mev/c, shows a reduction in the (g.s./4 Mev) ratio at the detector angles, suggesting that the recoil anisotropy is correlated with the proton direction. Because the protons are identical particles we constrained our T matrix to be symmetric in the exchange of the two protons. [Note that the second term in Eq. (2) also satisfies this symmetry condition since $\cos\theta_1' = \cos\theta_2'$.] Furthermore, if the T matrix is a smoothly varying function of the kinematic variables, the anisotropy must go to zero as the recoil momentum goes to zero thereby giving a (P_R) dependence. All of this led to the functional form

$$g(\theta_R,\phi_R) = N(P_R)\times[1+B(P_R)(\hat{\mathbf{P}}_R\cdot\hat{\mathbf{P}}_1)(\hat{\mathbf{P}}_R\cdot\hat{\mathbf{P}}_2)] \times[1+C(P_R)\cos\theta_R] , \quad (3)$$

where the last factor (discussed in the following) comes from the quasideuteron model and the three parameters N, B, and C depend upon the magnitude of P_R. B and C are chosen to fit the data and $N(P_R)$ is included to remove the P_R dependence from the integral of $g(\theta_R,\phi_R)$ over θ_R,ϕ_R,

$$\int g(\theta_R,\phi_R)d\Omega_R = \text{constant (independent of } P_R) . \quad (4)$$

This condition is necessary since we wish to constrain $g(\theta_R,\phi_R)$ so that the form factor $f(P_R)$ gives the angle-averaged dependence of $|T|^2$ upon P_R. In actuality, to keep things simple, we do not exactly satisfy Eq. (4). Instead we set $N(P_R)$ as

$$N(P_R) = 1/[1-B(P_R)/3] . \quad (5)$$

This is the value of $N(P_R)$ satisfying Eq. (4) if the opening angle between the two protons is 180°, $\hat{\mathbf{P}}_1\cdot\hat{\mathbf{P}}_2 = -1$.

The last term in Eq. (3), using the quasideuteron model, comes from the energy dependence of the ^{2}H(π^+,2p) reaction. The sum of the two proton energies in their c.m. frame in the ^{16}O(π^+,2p)^{14}N reaction depends upon the kinematic variables P_R and θ_R in the approximate form $[1+C(P_R)\cos\theta_R]$. The known energy dependence[15] of the ^{2}H(π^+,2p) reaction near $T_\pi = 60$ MeV is approximated by

$$\frac{d\sigma_{\text{lab}}}{dT_\pi(\text{lab})} = 0.07 \text{ mb/MeV} . \quad (6)$$

To explain how this energy dependence results in a θ_R dependence, we describe the following situation. If the $A=14$ residual nucleus recoils with momentum $\mathbf{P}_R$ parallel to $\mathbf{P}_\pi$ ($\theta_R = 0$), then according to the quasideuteron model the quasideuteron (pn) pair in the ^{16}O target nucleus has the opposite momentum, $-\mathbf{P}_R$, antiparallel to the pion momentum. This situation results in a higher center-of-mass energy of the πNN subsystem resulting in a larger pion absorption cross section. Similarly, if the recoil momentum $\mathbf{P}_R$ is antiparallel to $\mathbf{P}_\pi$, the situation results in a lower center-of-mass energy of the πNN subsystem and a smaller pion absorption cross section. Using the energy dependence of Eq. (6), we can calculate the θ_R dependence predicted by the quasideuteron model,

$$C(P_R) = 7.710^{-4}\times P_R , \quad (7)$$

where P_R is in units of MeV/c. In the present analysis we let $C(P_R)$ vary to fit the data and observe how close it comes to the predicted value. Our fits give values of $C(P_R)$ which are consistent with the quasideuteron prediction but the errors on the $C(P_R)$ parameter are comparable to its magnitude. Because of the poor precision we choose to remove $C(P_R)$ as a free parameter and fix it to the quasideuteron value [Eq. (7)].

In summary, the functional form of the T matrix is chosen based upon the quasideuteron model and the examination of our data. This gives a reasonable description of the data. Our complete data set covers the following phase space: $26.5 < T_1 < 160$ MeV; $24 < T_2 < 118$ MeV; $265.5° < \phi_1 < 274.5°$; $85.5° < \phi_2 < 94.5°$; and four sets of (θ_1,θ_2) angles whose centroids were given earlier and which have an angular spread of 24° for each detector angle. However, because much of this 24° angle spread in both θ_1 and θ_2 was due to the large beam size on target, the angles θ_1 and θ_2 are correlated and are constrained over a much smaller angular range relative to each other. This constraint is best described by the following statement: θ_1 evaluated in the center of momentum of the two protons could vary by only ±4.5° about its central value for each of the four sets of angles. The polar angles are all defined using the coordinate system in Fig. 1. The phase space of our data is now completely defined and fits to our measured triple-differential cross sections within this phase space region can be calculated using the T matrix. Any uncertainty in the T matrix only enters when we extrapolate to unmeasured regions of phase space.

IV. THE EXTRACTION OF THE T MATRIX

The form factors do not have any prescribed functional form except that they be relatively smooth. Their shape is

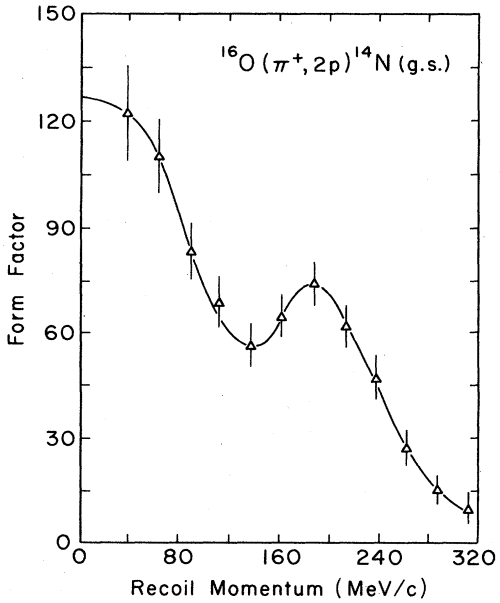

FIG. 4. The $^{16}O(\pi^+,2p)^{14}N$ ground state form factor. The solid line is the T matrix used in the Monte Carlo code. The data points are the raw data with the remaining part of the T matrix and the detector phase space acceptance factored out. The error bars are statistical.

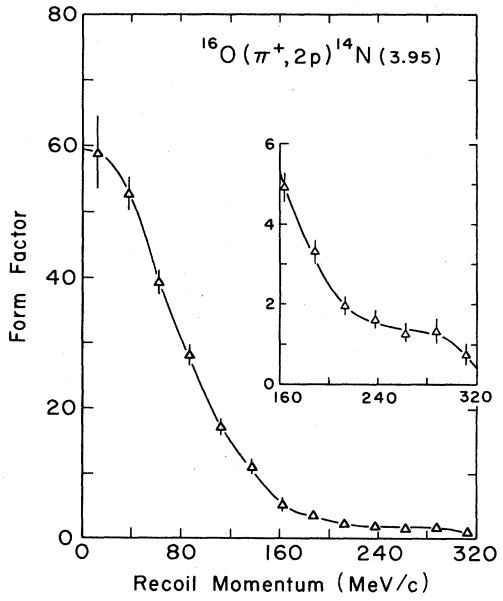

FIG. 5. The $^{16}O(\pi^+,2p)^{14}N$ 3.95 MeV form factor, $f(P_R)$. The solid line is the T matrix used in the Monte Carlo code. The data points are defined as in Fig. 2.

determined by the recoil momentum distribution of the data. The extracted form factors of the T matrices for the ^{14}N 1^+ ground state and 1^+ 3.95 MeV state are shown in Figs. 4 and 5. Both transitions show an enhancement at zero recoil momentum. This is characteristic of an $L=0$ angular momentum transfer. The data points are experimental yields at each momentum corrected for the detection efficiency and with the remaining T matrix and three-body phase space factored out of the yield. The error bars are only statistical. The surprising feature of Fig. 4 is that the ^{14}N ground state transition appears to have a large $L=0$ component. Other reactions which remove a (pn) pair from ^{16}O, for example, the (p,^{3}He) and (d,^{4}He) reactions,[13,24] show no noticeable $L=0$ component, but rather a dominant $L=2$ component. These stripping reactions predominantly select a (pn) pair in a relative s state, $l=0$, and the experimental results from these (pn) pickup reactions agree with the predictions of Cohen and Kurath.[16] Neither l nor L are good quantum numbers in the ^{16}O wave function but are strongly coupled to each other. If the $(\pi^+,2p)$ reaction involves pion absorption on an excited virtual (pn) cluster[17] with $l\neq 0$, then the L distribution, as shown in the form factor, will be quite different from the L distribution in a (p,^{3}He) or (d,^{4}He) reaction. This is a likely explanation of the large $L=0$ component in the ground state form factor. The 3.95 MeV transition has a dominant $L=0$ distribution in agreement with other reactions. The half-width at half-maximum of this form factor is about 80 MeV/c, which is in approximate agreement with theoretical calculations.[17]

The $L=2$ component of the form factors is predicted to peak at about 225 MeV/c. A rise is observed in the ground state form factor at about 180 MeV/c and a hint of an enhancement in the 4 MeV form factor near 240 MeV/c. We suspect that these structures in the form factors are associated with the $L=2$ component, but we do not know why they are shifted away from 225 MeV/c. To contrast these form factors with what could be expected from the quasideuteron model, consult the calculations of Ref. 17.

The additional (θ_R,ϕ_R) dependence in the T matrix, not predicted by the quasideuteron model, is given by the $B(P_R)$ parameter shown in Fig. 6. To understand how we

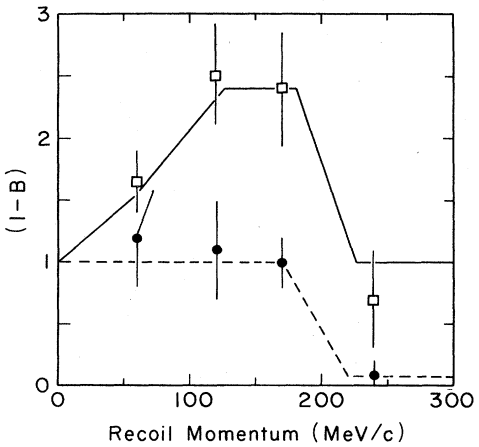

FIG. 6. A plot of $1-B(P_R)$ against recoil momentum. The solid line (4 MeV state) and dashed line (ground state) give the values used in the T matrix. The squares and dots are the values obtained from least squares fits to the recoil angular distributions of the 4 MeV and ground state, respectively. The error bars are defined in the text.

TABLE I. Regions of enhanced detection efficiency.

(θ_1,θ_2)	θ_1'	$(\hat{\mathbf{p}}_R\cdot\hat{\mathbf{p}}_1)(\hat{\mathbf{p}}_R\cdot\hat{\mathbf{p}}_2)$	$\cos\theta_R$	Region of beam
60°,103°	63°–72°	−0.95	±0.5	Center
60°,80°	74°–83°	$\geq(-0.25)$	−1.0	Left edge
80°,100°	75°–83°	$\geq(-0.25)$	+1.0	Right edge
100°,100°	87°–93°	$\geq(-0.25)$	+1.0	Right edge

obtained the values of this parameter, it is important to know the kinematic regions of enhanced detection efficiency listed for each of the four pairs of detector angles in Table I. The second, third, and fourth columns in the table list the values of three of the kinematic expressions appearing in the T matrix where the detection efficiency is greatly enhanced. The (60°,103°) data are dominated by events with $(\hat{\mathbf{P}}_R,\hat{\mathbf{P}}_1)(\hat{\mathbf{P}}_R,\hat{\mathbf{P}}_2)$ near the value of −0.95, whereas the data at the other three pairs of angles are dominated by events with $(\hat{\mathbf{P}}_R,\hat{\mathbf{P}}_1)(\hat{\mathbf{P}}_R,\hat{\mathbf{P}}_2)$ closer to zero. $B(P_R)$ multiplies $(\hat{\mathbf{P}}_R,\hat{\mathbf{P}}_1)(\hat{\mathbf{P}}_R,\hat{\mathbf{P}}_2)$ in the T matrix, and it is found that a nonzero value of $B(P_R)$ is needed to bring the (60°,103°) data set into agreement with the other three data sets. In particular the (60°,103°) yield to the ^{14}N ground state is abnormally low above recoil momentum of 200 MeV/c and the (60°,103°) yield to the 4 MeV state is abnormally high near a recoil momentum of 150 MeV/c. The Monte Carlo code could simulate these results using the $B(P_R)$ values plotted by the lines in Fig. 6. With these values of $B(P_R)$ the data sets at each of the four pairs of detector angles gave the identical form factors shown in Figs. 4 and 5.

Figure 6 is a plot of $(1-B)$. The requirement that $|T|^2$ be positive-definite places an upper bound on B of 1. Values of $(1-B)$ greater than 1 imply an enhanced collinearity in which the recoiling nucleus preferentially moves parallel to one of the proton momenta. Values of $(1-B)$ less than 1 imply a depressed collinearity in which the recoiling nucleus preferentially moves perpendicular to the proton momenta. The ground state and 4 MeV transitions show very different recoil angular distributions. The ground state has a depressed collinearity at large recoil momenta, whereas the 4 MeV transition has an enhanced collinearity yield between P_R equal to 100 and 200 MeV/c.

Another method of obtaining the $B(P_R)$ parameter is to add up the data sets at all four pairs of detector angles, separate the data into several regions of P_R, plot each yield vs θ_R, and apply a least squares fit to the data. Examples of the angular distributions vs θ_R are shown in Fig. 7 for the ground state transition with recoil momentum between 140 and 300 MeV/c and in Fig. 8 for the 4 MeV transition with recoil momentum between 100 and 200 MeV/c. The solid lines in Figs. 7 and 8 are not the least-squares fits but rather the predictions of the Monte Carlo simulation using the $B(P_R)$ obtained by making the (60°,103°) data set agree with the other data sets. The values of $B(P_R)$ corresponding to the best chi-squared fits to the angular distributions are shown as the points with error bars in Fig. 6. The chi-squared per degree of freedom, x^2/ν, is typically between 1.0 and 1.5 for each of the best fits with $\nu=11$. The error bar associated with each point in Fig. 6 is the range of values of $B(P_R)$ for which the x^2/ν stays within 0.5 of its minimum value. This definition of the error was based upon the shape of

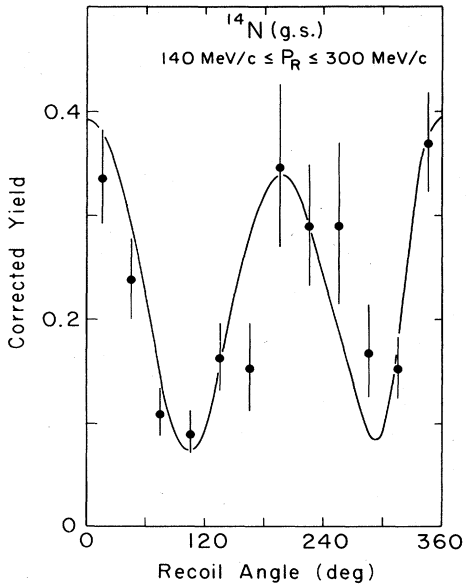

FIG. 7. The recoil angular distribution of the ground state for recoil momenta between 140 and 300 MeV/c. The data points are sums of the data collected at all four pairs of detector angles and divided by the equivalent Monte Carlo yield calculated with a T matrix isotropic in (θ_R,ϕ_R). The solid line gives the Monte Carlo calculation with the (θ_R,ϕ_R) dependence put into the T matrix divided by the same Monte Carlo calculation with the (θ_R,ϕ_R) dependence removed. The errors are statistical.

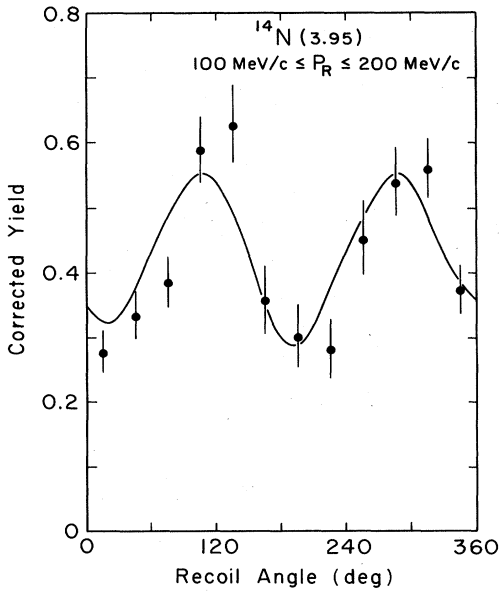

FIG. 8. The same type of recoil angular distribution as in Fig. 7, except for the 4 MeV state with recoil momentum between 100 and 200 MeV/c.

the x^2/ν vs $B(P_R)$ distribution and was chosen to give a good measure of the uncertainty in the B parameter.

The best fit to the recoil angular distributions generally becomes worse as the anisotropy becomes larger. The worst chi-squared is about 2.5, occurring for the 4 MeV transition at recoil momenta between 100 and 200 MeV/c. The observation that the minimum chi-squared increases as the anisotropy increases is an indication that the functional form for the T matrix is not perfect. The examination of Figs. 7 and 8 reveals some of the differences. The oscillatory pattern in the data appears to be shifted slightly relative to the Monte Carlo simulation.

Up to this point, all the errors presented in the paper have been statistical. There are also a few systematic errors. The potentially most severe systematic error in the extraction of the $B(P_R)$ parameter is due to uncertainties in the beam distribution on the target. The horizontal width of the beam is 2.7 cm FWHM and with the target normal at 70 deg relative to the beam, the beam had a spread of 8 cm across the target. Because of the phase space acceptance of the proton detectors, there was a strong correlation between the recoil angle, θ_R, of a detected $(\pi^+,2p)$ event and the position of the event on the target. This correlation is presented in the last three columns of Table I. If the wrong beam distribution is inserted into the Monte Carlo code, errors will appear in the extracted recoil angular distributions. Fortunately the beam distribution was monitored very carefully during the experiment by periodically placing multiwire proportional chambers in the beam to measure both its spread and sometimes its angular divergence. Single protons were also detected continuously during each run and their projection back to the target gave a reasonable monitor of the beam distribution. The beam distribution remained constant with time. Very important was the procedure of normalizing the $^{16}O(\pi^+,2p)$ data with the $^2H(\pi^+,2p)$ data. The $^2H(\pi^+,2p)$ data were also sensitive to the beam distribution. Therefore, the procedure of normalizing to the $^2H(\pi^+,2p)$ data removed first-order errors due to incorrect beam widths and centroids. In conclusion, we believe that systematic errors were kept to a minimum and are smaller than the statistical errors.

The remaining parameter in the T matrix is a_2, which multiplies $P_2(\cos\theta_1')$. The first column in Table I shows the range of values of θ_1' covered in our data. The (100°, 100°) data set, which covers the largest values of θ_1', is not so useful for studying the a_2 parameter because there are no $^2H(\pi^+,2p)$ events in this data set to fix precisely the normalization and remove systematic errors. Therefore, we are primarily limited to the range of angles 63° to 83°. The main problem with our data is that the detector angles were not chosen to differentiate easily between the $P_2(\cos\theta_1')$ dependence and the $(\hat{\mathbf{P}}_R,\hat{\mathbf{P}}_1)(\hat{\mathbf{P}}_R,\hat{\mathbf{P}}_2)$ dependence in the T matrix. As shown in Table I the data set covering the angular range $\theta_1'=63°\rightarrow72°$ has events with $(\hat{\mathbf{P}}_R,\hat{\mathbf{P}}_1)(\hat{\mathbf{P}}_R,\hat{\mathbf{P}}_2)$ near -0.95, whereas the data sets corresponding to $\theta_1'=75°\rightarrow83°$ have events with $(\hat{\mathbf{P}}_R,\hat{\mathbf{P}}_1)(\hat{\mathbf{P}}_R,\hat{\mathbf{P}}_2)$ predominantly larger than -0.25. This results in a strong correlation between the values of the $B(P_R)$ and a_2 parameters extracted from the data. This correlation does not present any ambiguity in a_2 and $B(P_R)$ at $P_R=0$ because of the necessary requirement that $B(P_R=0)=0$. To avoid serious ambiguities in these parameters at nonzero values of P_R, we choose a_2 to be independent of P_R. This is a valid assumption according to the quasideuteron model. If incorrect, the assumption will lead to sizable errors when extrapolating to the unmeasured regions of phase space. By fitting the data we obtain the following a_2 values:

$$a_2=0.88\pm0.3 \text{ for ground state},$$

$$a_2=1.17\pm0.1 \text{ for 4 MeV state}.$$

These values are consistent with the value $a_2=1.09$ for the $^2H(\pi^+,2p)$ reaction. Therefore, we set the a_2 value equal to 1.09 for each transition and used this value of a_2 in the extraction of $B(P_R)$ given earlier.

In summary, the parameters $C(P_R)$ and a_2 were initially varied to examine the consistency of our data with the quasideuteron model prediction of these parameters. The data were found to be consistent with the model prediction of these two parameters. To reduce the number of variables, these two parameters were held fixed at the values predicted by the model. In the final fit to the data only the form factor and the $B(P_R)$ parameter, both with an arbitrary functional form, were allowed to vary.

V. CROSS SECTIONS

In order to calculate triple-differential cross sections using the functional form of the T matrix given in Sec. IV, an overall normalization is required. A comparison of the experimental yields and Monte Carlo detection efficiencies for both the $^2H(\pi^+,2p)$ and $^{16}O(\pi^+,2p)$ reactions allows us to extract cross sections for each $^{16}O(\pi^+,2p)^{14}N$ transition. The procedure is as follows.

A solid angle somewhat larger than one of the proton detectors is defined and all events within this solid angle are simulated. The percentage of these events in which both protons are detected gives the detection efficiency. The size of this solid angle is not critical (i.e., will not change the final result) as long as it is large enough to include all possible coincident events. The experimentally measured yield is divided by the integrated beam, target thickness, computer live time, and also by the solid angle of the simulation and the corresponding detection efficiency. The resulting quotient is proportional to a single-differential cross section. Since the single-differential cross section of the $^2H(\pi^+,2p)$ reaction is known, the constant of proportionality is obtained from the $^2H(\pi^+,2p)$ data. This constant of proportionality can be used to get the single-differential cross section for any $^{16}O(\pi^+,2p)^{14}N$ transition if the T matrix is known. Even more important is that this constant of proportionality can be used to normalize uniquely the T matrix for each transition. An advantage of using this T-matrix formalism to extract cross sections is that we know how the single-differential cross section, $d\sigma/d\Omega_1$, is varying over the solid angle, Ω_1, of simulation in the Monte Carlo code and we can account for this variation in our normalization procedure. This is important because the large beam spread on target results in a large spread in θ_1 of $\pm12°$. The solid angle used in the simulation must include this full angular spread.

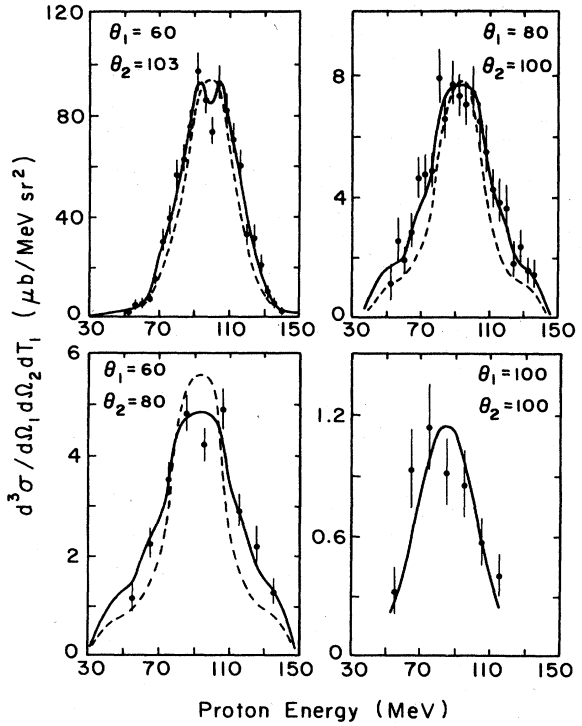

FIG. 9. The triple-differential cross sections of the transition to the 4 MeV state for the four pairs of central detector angles used in the experiment. In all cases, $\phi_1=270°$ and $\phi_2=90°$. The data points are defined in the text. The solid line is the TRIDIF calculation using the full T matrix described in the text. The dashed line is the TRIDIF calculation with the $B(P_R)$ parameter set to zero, and is arbitrarily normalized.

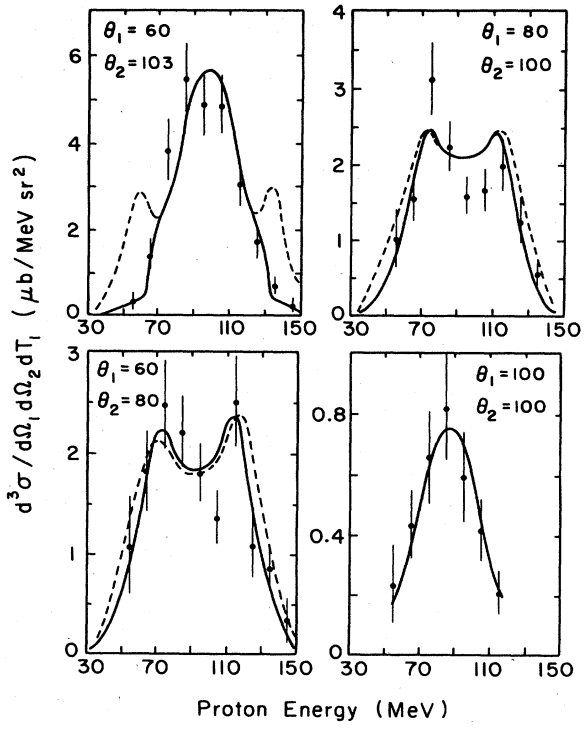

FIG. 10. Triple-differential cross sections of the transition to the ground state. The format is identical to Fig. 9.

Normally, if the solid angle is small enough, the procedure is to assume that the single-differential cross section is constant over the full solid angle. We cannot make this assumption without introducing a sizable error in the normalization.

Once the T matrix is normalized, all the ingredients exist to present the experimentally measured triple-differential cross sections. As long as we restrict ourselves to the phase space covered by the detectors, the model dependence in the T matrix will have a negligible effect on the triple-differential cross sections. These cross sections can be considered to be model-independent measurements. The model dependence only enters when the T matrix is extrapolated to an unmeasured region of phase space. We have written a code TRIDIF, which takes the T matrix for a particular transition and calculates any triple-differential cross section, or double- or single-differential cross section.

Some of our measured triple-differential cross sections are shown in Figs. 9 and 10. The data points in each figure are

$$\frac{\text{Data yield at } E_1}{\text{Monte Carlo yield at } E_1} \times \frac{d^3\sigma(\text{TRIDIF})}{d\Omega_1 d\Omega_2 dT_1} ,$$

where both the Monte Carlo and TRIDIF computer codes use the same T matrix. The normalized T matrix determines the cross section (solid line) and the data points with statistical errors reveal how well the Monte Carlo code with this T matrix reproduces the energy distribution of the data. We also show the shape of the cross section (dashed line) which one would obtain if the $B(P_R)$ parameter in the T matrix is set equal to zero. The T matrix with the $B(P_R)$ term removed is not properly normalized so that the magnitude of the dashed lines in the figures is meaningless. Only the shape of the dashed lines is of interest.

Figure 9 shows the triple-differential cross sections of the 4 MeV 1^+ state at each pair of detector angles used in the experiment. As the figure reveals, the T matrix is successful in reproducing the data. If the $B(P_R)$ parameter is turned off, the T matrix gives a significantly different dependence of the triple-differential cross section upon proton energy. For example, the $B(P_R)$ term in the T matrix gives a double hump near 100 MeV in the (60°, 103°) triple-differential cross section. This double hump agrees well with the data. In general, the $B(P_R)$ dependence of the 4 MeV state broadens out the triple-differential cross sections over a wider energy range. However, the shape of the triple-differential cross section is primarily determined by the form factor. If the only piece of evidence which we examine in our data is the proton energy distributions shown in Fig. 9, then the elimination of the $B(P_R)$ parameter could be partially compensated with a widening of the form factor. This correlation between $B(P_R)$ and the form factor was found to be very weak when the data was studied in its full detail. It is res-

trictive to project out of the data a few select triple-differential cross sections as shown in Fig. 9 and reveal only a small part of our multidimensional data. There is no simple way to display all of our data in their full complexity and, therefore, we have defined a T matrix which contains all of the details.

The full T matrix is given by the $C(P_R)$ [Eq. (7)]; the $a_2(=1.09)$ parameters predicted by the quasideuteron model, $f(P_R)$; and the $B(P_R)$ functions plotted in Figs. 4–6. The normalization of the T matrix can be obtained using any of the cross sections quoted in the following.

Figure 10 shows the triple-differential cross sections of the ground state at each pair of detector angles used in the experiment. The display format is identical to the format used in Fig. 9. The Monte Carlo code (with the ground state T matrix) reproduces the energy distributions of the data reasonably well. The reproduction of these energy distributions is destroyed if the $B(P_R)$ parameter is set equal to zero (dashed lines). Since the $B(P_R)$ parameter has the opposite sign for the ground state as for the 4 MeV state, it has the opposite effect on the energy distributions. The $B(P_R)$ parameter used in the ground state T matrix narrows the energy distribution of the triple-differential cross section. The $B(P_R)$ parameter has a very dramatic effect on the (60°,103°) triple-differential cross section. The structure of the ground state form factor (Fig. 4) results in enhancements of the (60°,103°) triple-differential cross sections at proton energies of 60 and 135 MeV. However, the very strong $B(P_R)$ parameter in the T matrix significantly changes the shape of the triple-differential cross section. The enhancements near 60 and 135 MeV become depressions when the $B(P_R)$ parameter is turned on, and these depressions are in agreement with the data.

Triple-differential cross sections select very precise regions of phase space. Our detectors covered a large continuous region of phase space. It is, therefore, reasonable to integrate one of the differentials in the triple-differential cross sections to obtain double-differential cross sections. These double-differential cross sections will involve an extrapolation into unmeasured regions of phase space as well as covering a larger portion of the detector phase space. If we choose our double-differential cross sections wisely, we can reduce the contribution from the extrapolation into unmeasured regions to a negligible amount.

The most conservative integration of the triple-differential cross sections is over the proton energy, T_1, since the detectors cover the energy region containing more than 95% of the yield. Performing this integration over proton energy we obtain the double-differential cross section shown in Fig. 11. These double-differential cross sections have both of the proton momentum vectors and the pion momentum vector in a common plane. Using the coordinate axis in Fig. 1, the angles are $\theta_1=60°$, $\phi_1=270°$, and $\phi_2=90°$. The double-differential cross sections are plotted vs θ_2. This can also be thought of as a yield variation with the opening angle between the two proton momenta. In this case the opening angle is $60+\theta_2$. No data points are shown because these cross sections involve an extrapolation. It should be emphasized

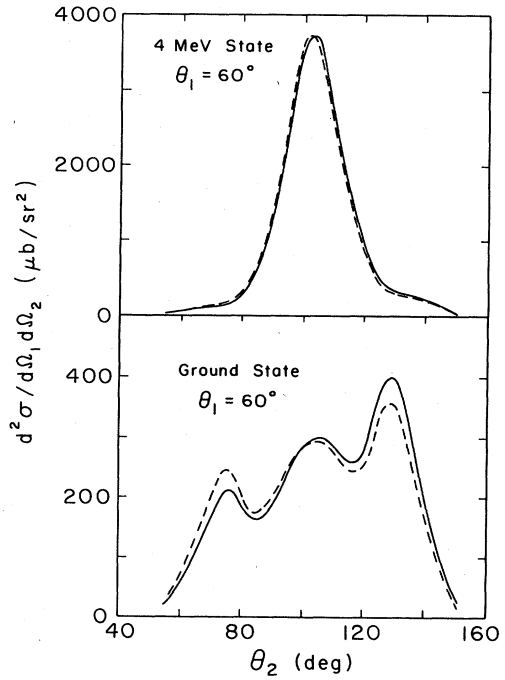

FIG. 11. Double-differential cross sections at $\theta_1=60°$, $\theta_1=270°$, and $\phi_2=90°$ calculated using TRIDIF with the full T matrix (solid lines) and with $C(P_R)$ set equal to zero (dashed lines).

that the T matrices for each transition give cross sections at all pairs of angles which are consistent with the data. Strictly speaking, our data only cover the range of θ_2 from 75° to 108° for the case $\theta_1=60°$. However, the double-differential cross section may be primarily a function of the opening angle between the two protons and our data cover nearly the full range of opening angles shown in Fig. 11.

The double-differential cross section plotted for the 4 MeV state in Fig. 11 has a full-width at half-maximum of about 22° which is approximately the same width as measured for the

$$^{16}\mathrm{O}(\pi^+,2\mathrm{p})^{14}\mathrm{N}(-2\leq E_x\leq 10\ \mathrm{MeV})$$

reaction at $T_\pi=70$ MeV.[7] The ground state's double-differential cross section is more diffusely spread over the opening angle with an effective width about three times the FWHM which is seen for the 4 MeV state. The cross sections of the 4 MeV state and ground state transitions at the central angle of 103° (corresponding to zero recoil momentum) are in the ratio of 12 to 1. The $C(P_R)$ parameter in the T matrix affects the centroid of the double-differential cross section. This $C(P_R)$ parameter, which is constrained to equal the value predicted by the quasideuteron model (see Sec. III), shifts the centroid about 2 deg from 102.7° to 104.9°, as shown for the 4 MeV transition in Fig. 11. Our data were not sensitive enough to verify this shift. We also show the double-differential cross sections with $C(P_R)$ set equal to zero (dashed lines in Fig. 11). The $C(P_R)$ parameter has a

larger affect upon the ground state's double-differential cross section with its more diffuse distribution.

The enhancement in the ground state's double-differential cross section at $\theta_2=75$ and 130° in Fig. 11 comes from the enhancement in the ground state's form factor near 180 MeV/c (Fig. 4). The $B(P_R)$ parameter also affects the shape of the θ_2 dependence of the double-differential cross section. A negative value of $B(P_R)$ for the 4 MeV state makes its double-differential cross section narrower and a positive value of $B(P_R)$ for the ground state's T matrix leads to a broader distribution.

If the triple-differential cross sections are integrated over $d\Omega_2$, another type of double-differential cross section, $d^2\sigma/d\Omega_1 dT_1$, is obtained. These are shown for the 4 MeV and ground state transitions in Fig. 12, plotted against T_1. These cross sections involve a considerable extrapolation of the T matrix because the solid angles of our proton detectors cover regions containing less than half of the yield of these double-differential cross sections. The major extrapolation is in the ϕ direction. Our detectors each covered a range of about 9 deg in the ϕ direction which by cylindrical symmetry arguments covers a full 18 deg of the angular correlation in the ϕ direction. This angular range was considerably smaller than the angular range covered in the θ direction. The shape of $d^2\sigma/d\Omega_1 dT_1$ is very similar for both the 4 MeV and ground state transitions. The ground state transition is slightly broader. The ratio of these double-differential cross sections near the maximum, $T_1=95$ MeV, are in the ratio of 2.5 to 1 which is a much smaller ratio than for the double-differential cross sections in Fig. 11.

The triple-differential cross sections can be integrated over both $d\Omega_1$ and dT_1 to obtain the single-differential cross section, $d\sigma/d\Omega_1$. This single-differential cross section involves the sum of the extrapolations needed to obtain the two types of double-differential cross sections in Figs. 11 and 12. The single-differential cross sections which we obtain at $\theta_1=60°$ in the laboratory reference frame are

$$\frac{d\sigma}{d\Omega_1}=\begin{cases}0.36\text{ mb/sr (ground state)},\\ 0.845\text{ mb/sr (4 MeV state)}.\end{cases}$$

The ground state cross section is about 42 percent of the elementary ^{2}H(π^+,2p) laboratory cross section at 60 deg. The 4 MeV cross section is about 98 percent of the elementary cross section. It should be remembered that all of the cross sections are normalized to the known elementary ^{2}H(π^+,2p) cross section. In addition to the errors associated with the extrapolation of the T matrix into an unmeasured region, there is also approximately ±10 percent overall normalization error.

The ratio of the ground state to the 4 MeV state cross section is 0.43 which is approximately equal (within experimental error) to the ratio of cross sections to these states measured in the ^{16}O(p,pd)^{14}N reaction.[18] This could be construed as evidence for the quasideuteron model in which the pion is selecting a (pn) pair in a $^3S_1$ configuration.

The angular distributions of the single-differential cross sections of the ground state and 4 MeV state are approximately the same as the angular distribution of the ^{2}H(π^+,2p) reaction. This similarity occurs because the θ_1' dependence, given by the a_2 parameter, was found to be nearly identical for the three cases (see Sec. IV). It is not unreasonable to assume the angular distributions are also identical, over the unmeasured phase space, and integrate over $d\Omega_1$. When integrating over the 4π solid angle, the resulting total cross section must be divided by two because of the two identical protons in the final state. The total integrated cross sections which we obtain for each transition are

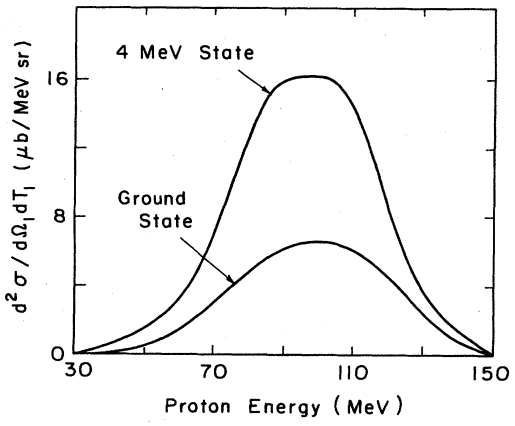

FIG. 12. Double-differential cross sections at $\theta_1=60°$ calculated using TRIDIF with the full T matrix.

$$\sigma(\text{ground state})=2.9\text{ mb},$$

$$\sigma(4\text{ MeV state})=6.7\text{ mb}.$$

It is interesting to compare these cross sections to the total absorption cross section of π^+ on ^{16}O at 60 MeV. Total absorption cross sections have been measured on ^{12}C and other nuclei at $T_\pi=50$ MeV (Ref. 19) and at $T_\pi=85$ MeV (Ref. 20). Interpolating both the energy and mass dependence of the total absorption cross section from these two references, we estimate that the total absorption cross section of π^+ on ^{16}O at 60 MeV is 130 mb. This total absorption cross section divided into the total cross sections for each 1^+ transition gives 2.2% for the ground state transition and 5.2% for the 4 MeV state transition. The percentage of the absorption rate going to the 4 MeV state has been measured with stopped π^- to be (2.5±0.7)%, 1.8%, or (4.8±0.9)% (see Ref. 12). Our value of 5.2% for the 4 MeV state is slightly larger than the stopped π^- measurements.

VI. SUMMARY

The data given in this paper represent the first measured absolute triple-differential cross sections to discrete states in the (π^+,2p) reaction on a target with atomic mass greater than three. Although the form of the T matrix predicted from a quasideuteron absorption process can describe many features of the data, there are two major modifications of the T matrix which are necessary to explain the data. Firstly, the ^{14}N 1^+ ground state form fac-

tor shows a large $L=0$ component. This is in dramatic contrast with the well-known nuclear structure in which a proton-neutron pair in a $^3S_1$ quasideuteron state is coupled by $L=2$ relative angular momentum with the ^{14}N ground state to form the ^{16}O ground state. Secondly, the T matrix for transitions to both of the ^{14}N 1^+ states shows a strong dependence upon recoil angle. The ^{14}N(4 MeV) 1^+ nucleus with momentum near 150 MeV/c has an enhanced probability of recoiling parallel to one of the two proton momenta, whereas the ^{14}N(g.s.) 1^+ nucleus at large recoil momentum has a momentum distribution enhanced in the direction perpendicular to the proton momenta. The differences in these two 1^+ transitions must be due to nuclear structure effects. It is well known that the 4 MeV 1^+ state is primarily $(P_{1/2}^{-1}P_{3/2}^{-1})_1$ and the ground state is primarily $(P_{1/2}^{-2})_1$. This data should thus make feasible a detailed theoretical study of the $(\pi^+,2p)$ reaction mechanism. An initial attempt[21] using an isobar-doorway model has been made to study the ^{16}O$(\pi^+,2p)$ reaction, but this model has not been fully developed.

The ^{16}O$(\pi^+,2p)^{14}$N data extend over a large enough region of phase space that it was possible to study and specify many detailed features of the T matrix for the two 1^+ transitions. Although the functional form of the T matrix cannot be uniquely determined and there is ambiguity because of cross correlations in some of the parameters, we feel that the T matrices which we extracted are realistic and can, with some reliability, be extrapolated into unmeasured regions of phase space. Extrapolating over the full phase space, we find that 7.3% of the pion absorption cross section is contained in the ground state plus the 4 MeV state transitions. The most severe extrapolation in obtaining the total integrated cross section is the integration over $d\Omega_1$, the solid angle of one of the protons, after the solid angle of the other proton has already been integrated over. This extrapolation is essentially an integration of the single-differential cross section, $d\sigma/d\Omega_1$. This is a severe extrapolation because our data do not extend forward of 63° in the center-of-mass frame of the two protons. However, we feel that this extrapolation, assuming the same θ_1 angular dependence as the ^{2}H$(\pi^+,2p)$ reaction, is likely to be accurate. Firstly, the data from the two 1^+ states indicate angular distributions nearly identical to the elementary ^{2}H$(\pi^+,2p)$ angular distributions for angles larger than 63° in the center-of-mass frame. Secondly, other studies of the $(\pi^+,2p)$ reaction on neighboring targets and at a variety of pion energies invariably show angular distributions consistent with the elementary ^{2}H$(\pi^+,2p)$ reaction. For example, the ^{12}C$(\pi^+,2p)$ reaction at $T_\pi=165$ and 245 MeV shows angular distributions consistent with the elementary ^{2}H$(\pi^+,2p)$ angular distribution to the most forward measured angle, 30°, in the center of mass of the two protons.[22]

The only other major extrapolation in the extraction of the total cross section for each 1^+ transition is the extrapolation in the azimuthal angle, ϕ. This extrapolation corresponds to holding the azimuthal angle of one proton, ϕ_1, fixed and integrating over the azimuthal angle of the other proton, ϕ_2. Our data cover an effective range in ϕ of 18° which, we estimate, contains almost half of the yield. We do not know how good the ϕ extrapolation is. We obtain the value of 5.2% for the fraction of the absorption cross section populating the ^{14}N(4 MeV) state, whereas the stopped π^- data get a smaller fraction with measurements varying from 1.8% up to 4.8%.[12]

Looking at our ^{16}O$(\pi^+,2p)^{14}$N spectra in Fig. 2, it becomes apparent that the ground state and 4 MeV state carry only a minor fraction of the total $(\pi^+,2p)$ yield. If the extrapolation of the T matrix is correct in giving 7.3% of the absorption cross section to the ground state and 4 MeV state, then a sizable fraction of the total pion absorption cross section must be feeding into other $(\pi^+,2p)$ channels. Altman *et al.*[22] claim that their ^{12}C$(\pi^+,2p)$ data at $T_\pi=165$ MeV indicate that only about 10% of the total absorption cross section can be attributed to a one-step quasideuteron $(\pi^+,2p)$ process. If this statement also applies to the ^{16}O$(\pi^+,2p)^{14}$N reaction at $T_\pi=60$ MeV, then only a minor fraction of the $(\pi^+,2p)$ cross section can be associated with a one-step quasideuteron process. However, it should be pointed out that a different analysis[23] of the ^{12}C$(\pi^+,2p)$ data at $T_\pi=165$ MeV indicates that a larger fraction of the absorption cross section can be attributed to a one-step quasideuteron process.

Finally, we point out that considerable theoretical effort has been expended in studying the (π^+,p) or (p,π^+) reaction channels and very little theoretical work has gone to the study of the $(\pi^+,2p)$ channels. Because the $(\pi^+,2p)$ reaction is a much more dominant channel than is the (π^+,p) reaction, we hope that this very detailed data presented here will stimulate many theoretical investigations.

ACKNOWLEDGMENTS

We are grateful to the staff at LAMPF for their full cooperation and readiness to meet our special needs. We have profited from R. Pehl and his associates's expertise with germanium detectors. We are thankful for F. Megahan's careful attention to the everyday details of our experimental group.

*Permanent address: Physics Department, Wheaton College, Wheaton, IL 60187.

†Permanent address: Physics Department, University of New Mexico, Albuquerque, NM 87131.

‡Permanent address: Nuclear Physics Laboratory, University of Illinois, Champaign, IL 61820.

§Permanent address: Brookhaven National Laboratory, Upton, NY 11973.

**Permanent address: Physics Department, University of Pittsburgh, Pittsburgh, PA 15260.

††Present address: Lawrence Berkeley Laboratory, Berkeley, CA 94720.

[1]*Pion Production and Absorption in Nuclei—1981 (Indiana University Cyclotron Facility),* Proceedings of the Conference on Pion Production and Absorption in Nuclei, AIP Conf. Proc. No. 79, edited by R. D. Bent (AIP, New York, 1982).

[2]Symposium on Delta-Nucleus Dynamics, edited by T.-S. H. Lee, D. F. Geesaman, and J. P. Schiffer, Argonne National Laboratory Report Conf.-830588, 1983.

[3]*Mesons in Nuclei,* edited by M. Rho and D. Wilkinson (North-Holland, Amsterdam, 1979).

[4]I. Navon, E. Piasetzky, D. Ashery, A. Altman, G. Azuelos, F. W. Schleputz, and H. K. Walter, Phys. Lett. **95B**, 365 (1980).

[5]D. Koltun, Comments Nucl. Part. Phys. **11**, 171 (1983).

[6]G. A. Miller and L. S. Kisslinger, Phys. Rev. C **27**, 1669 (1983).

[7]E. D. Arthur, W. C. Lam, J. Amato, D. Axen, R. L. Burman, P. Fessenden, R. Macek, J. Oostens, W. Shlaer, S. Sobottka, M. Salomon, and W. Swenson, Phys. Rev. C **11**, 332 (1975).

[8]J. Favier, T. Bressani, G. Charpak, L. Massonnet, W. E. Meyerhof, and C. Zupancic, Nucl. Phys. **A169**, 540 (1971).

[9]K. G. R. Doss, P. D. Barnes, N. J. Collella, S. A. Dytman, R. A. Eisenstein, C. Ellegaard, F. Takeutchi, W. R. Wharton, J. F. Amann, R. H. Pehl, and A. C. Thompson, Phys. Rev. C **25**, 962 (1982).

[10]R. Rieder, P. D. Barnes, B. Bassalleck, R. A. Eisenstein, G. Franklin, R. Grace, C. Maher, P. Pile, J. Szymanski, W. R. Wharton, J. R. Comfort, F. Takeutchi, J. F. Amann, S. A. Dytman, and K. G. R. Doss (unpublished).

[11]P. D. Barnes, B. Bassalleck, R. A. Eisenstein, G. Franklin, R. Grace, C. Maher, P. Pile, R. Rieder, J. Szymanski, W. R. Wharton, J. R. Comfort, F. Takeutchi, J. F. Amann, S. Dytman, and K. G. R. Doss, Nucl. Phys. **A402**, 397 (1983).

[12]B. Bassalleck, H. D. Engelhardt, W. D. Klotz, C. W. Lewis, F. Takeutchi, H. Ullrich, and M. Furic, Nucl. Phys. **A343**, 365 (1980).

[13]A. Van Der Woude and R. J. De Meijer, Nucl. Phys. **A258**, 199 (1976).

[14]R. Liljestrand, G. Blanpied, G. W. Hoffmann, J. E. Spencer, and J. R. Rhodes, Nucl. Instrum. Methods **138**, 471 (1976).

[15]B. G. Ritchie, G. S. Blanpied, R. S. Moore, B. M. Preedom, K. Gotow, R. C. Minehart, J. Boswell, G. Das, H. J. Ziock, N. S. Chant, P. G. Roos, W. J. Burger, S. Gilad, and R. P. Redwine, Phys. Rev. C **27**, 1685 (1983).

[16]S. Cohen and D. Kurath, Nucl. Phys. **A141**, 145 (1970).

[17]N. F. Golovanova, I. M. II'in, V. G. Neudatchin, Yu F. Smirnov, and Yu M. Tchuvil'sky, Nucl. Phys. **A262**, 444 (1976).

[18]J. Y. Grossiord, M. Bedjidian, A. Guichard, M. Gusakow, J. R. Pizzi, T. Delbar, G. Gregoire, and J. Lega, Phys. Rev. C **15**, 843 (1977).

[19]I. Navon, D. Ashery, J. Alster, G. Azuelos, B. M. Barnett, W. Gyles, R. R. Johnson, D. R. Gill, and T. G. Masterson, Phys. Rev. C **28**, 2548 (1983).

[20]D. Ashery, I. Navon, G. Azuelos, H. K. Walter, H. J. Pfeiffer, and F. W. Schleputz, Phys. Rev. C **23**, 2173 (1981).

[21]W. R. Wharton and B. D. Keister, contribution to the Symposium on Delta-Nucleus Dynamics, edited by T.-S. H. Lee, D. F. Geesaman, and J. P. Schiffer, Argonne National Laboratory report, 1983.

[22]A. Altman, E. Piasetzky, J. Lichtenstadt, A. I. Yavin, D. Ashery, R. J. Powers, W. Bertl, L. Felawka, H. K. Walter, R. G. Winter, and J. V. D. Pluym, Phys. Rev. Lett. **50**, 1187 (1983).

[23]B. G. Ritchie, N. S. Chant, and P. G. Roos, Phys. Rev. C **30**, 969 (1984).